

Microscopic analysis of K^+ -nucleus elastic scattering based on K^+ -nucleon phase shifts

H. F. Arellano*

Departamento de Física, Facultad de Ciencias Físicas y Matemáticas, Universidad de Chile, Casilla 487-3, Santiago, Chile

H. V. von Geramb†

Theoretische Kernphysik, Universität Hamburg, Luruper Chaussee 149, D-22761, Hamburg, Germany

(Received 29 December 2004; published 29 August 2005)

We investigate K^+ -nucleus elastic scattering at intermediate energies within a microscopic optical model approach using the current K^+ -nucleon (KN) phase shifts from the Center for Nuclear Studies of the George Washington University as primary input. The KN phase shifts are used to generate Gel'fand-Levitan-Marchenko real and local inversion potentials. These potentials are supplemented with a short-range, complex separable term in such a way that the corresponding unitary and nonunitary KN S matrices are exactly reproduced. These KN potentials allow us to calculate all needed on- and off-shell contributions of the t matrix, the driving effective interaction in the full-folding K^+ -nucleus optical model potentials reported here. Elastic scattering of positive kaons from ${}^6\text{Li}$, ${}^{12}\text{C}$, ${}^{28}\text{Si}$, and ${}^{40}\text{Ca}$ are studied at beam momenta in the range 400–1000 MeV/c, leading to a fair description of most differential and total cross section data. To complete the analysis of the full-folding model, three kinds of simpler $t\rho$ calculations are considered and the results are discussed.

DOI: [10.1103/PhysRevC.72.025203](https://doi.org/10.1103/PhysRevC.72.025203)

PACS number(s): 13.75.Jz, 24.10.Ht

I. INTRODUCTION

Over the past two decades the study of K^+ -nucleus (KA) collisions with light targets received considerable attention both experimentally and theoretically [1–3] owing largely to the smooth energy dependence, the relative weak strength of the K^+ -nucleon (KN) interaction, and the strangeness of the projectile. Herewith, it was expected and largely confirmed that intermediate-energy $t\rho$ optical potentials would suffice to describe the scattering data. However, some unexpected and persistent shortcomings were observed in the description of total cross section data taken in transmission experiments at beam momenta in the range 500–1000 MeV/c [1,2,4]. This situation has triggered an outlook for new physics with models including unconventional as well as higher order effects [5,6]. Up to now an important and unsatisfactory element in all these discussions has been the absolute normalization error of the measured cross sections, being $\pm 17\%$ [3]. Among the various theoretical efforts we ought mention covariant formulations [3,6], considerations of medium modifications of the KN interaction within the target nucleus environment [7,8], the use of on- and off-shell t -matrix contributions with the construction of separable scattering amplitudes [9], and the possible manifestation of Θ^+ pentaquark in KA collisions [10].

The microscopic optical model potential (OMP) approach we present here embodies most of these elements but puts emphasis on the best possible direct use of KN phase-shift data to generate on- and off-shell KN t -matrix elements. This is achieved with the construction of a KN potential, in a true sense a KN optical model potential when the respective S matrix is nonunitary, which reproduces in absolute terms the phase-shift data. This approach distinguishes several steps. First,

for each partial wave and set of KN data, an optimal Gel'fand-Levitan-Marchenko inversion potential $V_\alpha(r)$ is calculated [11, 12]. Second, a short-range rank-one separable potential, with energy-dependent and possibly complex strengths is added to $V_\alpha(r)$ and matched to the data [12]. These potentials are used in Lippmann-Schwinger equations for the KN t matrix, the defined effective interaction in the full-folding optical model approach discussed here. These folding calculations are carried out in momentum space with the use of nonlocal single-particle target densities [13]. Herein, the full-folding calculations use only the KN t matrix and thus neglect the Pauli blocking in the propagation of nucleons in the nucleus.

The article is organized as follows. In Sec. II we specify the KN data and the KN effective interaction. In Sec. III we present the salient features of the full-folding KA optical potential and discuss three alternative $t\rho$ approximations. In Sec. IV we show and discuss KA elastic scattering applications for selected nuclei. In sec. V we present a summary and conclusions of this analysis.

II. THE KN EFFECTIVE INTERACTION

We base our study on the current KN partial-wave phase-shift single- and continuous-energy solutions for $0 < T_{\text{Lab}} < 1$ GeV of Richard Arndt *et al.* and retrieved data from the Center for Nuclear Studies (CNS) of the George Washington University (GWU) [14,15]. These data are sufficient to specify the partial-wave S matrix or t matrix on shell. However, these quantities alone are insufficient in the context of the many-body approach since the KA optical model requires the t matrix off shell. Thus, the problem is ill posed and requires a theoretical extension of the on-shell t matrix into the off-shell domain. The solution to this problem is not unique. However, since our analysis hinges upon a potential theory we chose a KN potential concept also for this purpose. The off-shell

*Electronic address: arellano@dfi.uchile.cl

†Electronic address: geramb@uni-hamburg.de

extension of the t -matrix interaction takes into account free-particle propagation, counted to all orders in the ladder approximation, but without KA medium effects. We calculate the t matrices with a Lippmann-Schwinger equation in momentum space.

A well-established and often-applied link between phase shifts and potential is the inverse scattering formalism of Gel'fand-Levitan and Marchenko. The present application points toward use of the fixed angular momentum or partial-wave Schrödinger-type equation version (mathematically, a Sturm-Liouville equation), yielding energy-independent and local potentials [11]. Before we enter into the more technical aspects of inversion it is useful to recall the relativistic aspects that we associate with the relative-motion Schrödinger-type equation being used for the KN pair in the center-of-momentum (c.m.) system.

The inversion method is useful and physically justified for cases in which the phase shifts are smooth functions of the energy and resonances are absent. However, actual KN phase-shift data are not perfectly smooth, show significant error bars, and are not free of personal preferences. To keep these preferences at a minimum we divide the KN partial-wave potentials into two parts. The first part is the result of a Gel'fand-Levitan-Marchenko inversion with an optimal smooth rational function fit to the unitary S -matrix sector of the data. The resulting real potentials are smooth functions of the radial distance and play the role of what we call a *reference potential*.

The basic equations of inversion are the radial Schrödinger equation

$$\left[-\frac{d^2}{dr^2} + \frac{\ell(\ell+1)}{r^2} + 2\mu V_\ell(r) \right] \psi_\ell(k, r) = k^2 \psi_\ell(k, r), \quad (1)$$

$$0 \leq r < \infty,$$

where $V_\ell(r)$ is a local, energy-independent but explicitly partial-wave-dependent coordinate space potential. The factor 2μ , the two-particle reduced mass, is used to make a comparison with nonrelativistic potentials more obvious. The right-hand side refers to the relative two-particle momentum or wave number k , which is related to the kinetic energy of the kaon in the laboratory system, T_{Lab} , its mass m_K , and the nucleon mass m_N , by means of

$$s = (m_N + m_K)^2 + 2m_N T_{\text{Lab}} \quad (2)$$

and

$$k^2 = \frac{s^2 + (m_K^2 - m_N^2)^2 - 2s(m_K^2 + m_N^2)}{4s}. \quad (3)$$

The boundary conditions for the physical solutions are

$$\lim_{r \rightarrow 0} \psi_\ell(k, r) = 0 \quad (4)$$

and

$$\lim_{r \rightarrow \infty} \psi_\ell(k, r) = \exp[i\delta_\ell(k)] \sin \left[kr - \frac{\ell\pi}{2} + \delta_\ell(k) \right]. \quad (5)$$

It is pertinent to mention that Eq. (1) is a true relativistic equation provided the right-hand-side eigenvalue corresponds to the square of the relativistic on-shell momentum. This is supported by works of Crater and collaborators [16,17]

on relativistic two-particle dynamics in the framework of Dirac's constraint dynamics, leading to a wave equation of the form $(\mathbf{p}^2 + \Phi(\mathbf{r}) - k^2)\psi = 0$. As a matter of convenience we express the interaction Φ as $\Phi(\mathbf{r}) = 2\mu V(r)$, with $1/\mu = 1/m_K + 1/m_N$.

The Gel'fand-Levitan and Marchenko inversions are two different algorithms that should yield exactly the same potential results. The use and comparison of both calculations guarantees robust results.

The experimental information enters in the Marchenko inversion via the partial-wave S matrix, which is related to the scattering phase shifts by the relation

$$S_\ell(k) = \exp[2i\delta_\ell(k)]. \quad (6)$$

We use a rational function interpolation and extrapolation of real data $\delta_\ell(k)$,

$$\delta_\ell(k) = \sum_{m=1}^M \frac{D_m}{k - d_m}, \quad (7)$$

with the asymptotic conditions

$$\lim_{k \rightarrow 0} \delta_\ell(k) \sim k^{2\ell+1} \quad \text{and} \quad \lim_{k \rightarrow \infty} \delta_\ell(k) \sim k^{-1}. \quad (8)$$

There are few poles d_m and strengths D_m sufficient to provide a smooth description of the data. For the KN system, there are no bound states to be extracted; thus we simply use a rational function interpolation and extrapolation of real data $\delta_\ell(k)$ with a fully symmetric distribution of poles and zeros in the upper and lower half k plane. This implies that the boundary conditions at the origin and at infinity are satisfied. Furthermore, using a symmetric Padé approximant for the exponential function guarantees that the number of zeros and poles of the S Matrix, in the upper and lower half complex k plane, are the same, the index is zero, and no bound states are present.

Using a [4/4] Padé approximation for the exponential function e^z is highly accurate and substituting the rational phase function into $z = 2i\delta_\ell(k)$ gives a rational S matrix

$$S_\ell(k) = 1 + \sum_{n=1}^{2N} \frac{s_n}{k - \sigma_n} = \prod_{n=1}^N \frac{k + \sigma_n^\uparrow}{k - \sigma_n^\uparrow} \cdot \frac{k + \sigma_n^\downarrow}{k - \sigma_n^\downarrow}, \quad (9)$$

where we denote $\{\sigma_n^\uparrow\} := \{\sigma_n | \text{Im}(\sigma_n) > 0\}$ and $\{\sigma_n^\downarrow\} := \{\sigma_n | \text{Im}(\sigma_n) < 0\}$. The Marchenko input kernel

$$F_\ell(r, t) = -\frac{1}{2\pi} \int_{-\infty}^{+\infty} h_\ell^+(kr) [S_\ell(k) - 1] h_\ell^+(kt) dk \quad (10)$$

is readily computed using Riccati-Hankel functions $h_\ell^+(x)$ and contour integration. This implies an algebraic equation for the translation kernel $A_\ell(r, t)$ of the Marchenko equation

$$A_\ell(r, t) + F_\ell(r, t) + \int_r^\infty A_\ell(r, s) F_\ell(s, t) ds = 0. \quad (11)$$

The potential is obtained from the translation kernel derivative

$$V_\ell(r) = -2 \frac{d}{dr} A_\ell(r, r). \quad (12)$$

Thus, the rational representation of the scattering data leads to an algebraic form of the potential.

The Gel'fand-Levitan inversion uses Jost functions as input. The latter is related to the S matrix by

$$S_\ell(k) = \frac{F_\ell(-k)}{F_\ell(k)}. \quad (13)$$

Using the representation (9), the Jost function in rational representation is given by

$$F_\ell(k) = \prod_{n=1}^N \frac{k - \sigma_n^\downarrow}{k + \sigma_n^\uparrow} = 1 + \sum_{n=1}^N \frac{B_n}{k + \sigma_n^\uparrow}, \quad (14)$$

or

$$|F_\ell(k)|^{-2} = 1 + \sum_{n=1}^N \frac{L_n}{k^2 - \sigma_n^{\downarrow 2}}. \quad (15)$$

The input kernel

$$G_\ell(r, t) = \frac{2}{\pi} \int_0^\infty j_\ell(kr) \left[\frac{1}{|F_\ell(k)|^2} - 1 \right] j_\ell(kt) dk, \quad (16)$$

where $j_\ell(x)$ represent the Riccati-Bessel functions, is analytic. The Gel'fand-Levitan equation

$$K_\ell(r, t) + G_\ell(r, t) + \int_0^r K_\ell(r, s) G_\ell(s, t) ds = 0 \quad (17)$$

relates input and translation kernels, where the potential is defined by

$$V_\ell(r) = 2 \frac{d}{dr} K_\ell(r, r). \quad (18)$$

Thus, this potential also has an algebraic form.

The second part is a short-range, rank-one separable potential with real or complex energy-dependent strengths fixed to the actual data. This idea has been developed and implemented in nucleon-nucleon studies and applied to nucleon-nucleus scattering [12,13]. Here, we use the KN potential as the sum of a local inversion potential $V_\alpha(r)$ supplemented with a separable term

$$V_{KN}(r, r', E) = V_\alpha(r') \frac{\delta(r - r')}{rr'} + \phi_\alpha(r) \Gamma_\alpha(E) \phi_\alpha(r'). \quad (19)$$

The partial waves are identified with α , and $\Gamma_\alpha(E)$ are energy-dependent strengths with imaginary component for those channels where the S matrix is not unitary. This is the case for only some partial-wave data. For a given reference potential $V_\alpha(r)$ and data, the determination of $\Gamma_\alpha(E)$ is a straightforward procedure [12].

Thus, we base the V_{KN} on the current solution of CNS/GWU- KN solutions [14,15]. All the used phase shifts, $L \leq 2$, are shown in Figs. 1–4. We distinguish different data: single-energy (full circles with error bars) and continuous-energy (dashed curves) solutions and the inversion reference potential phase shifts (solid curves), which reproduce the rational functions of the kinetic energy T_{Lab} . The isospin-zero ($I = 0$) stretched ($J = L + 1/2$) and antistretched ($J = L - 1/2$) channels are shown in Figs. 1 and 2, respectively. Similarly, the isospin-one ($I = 1$) stretched and antistretched channels are presented in Figs. 3 and 4, respectively. The corresponding inversion reference potentials are shown in Figs. 5 and 6. In these figures we observe that all potentials

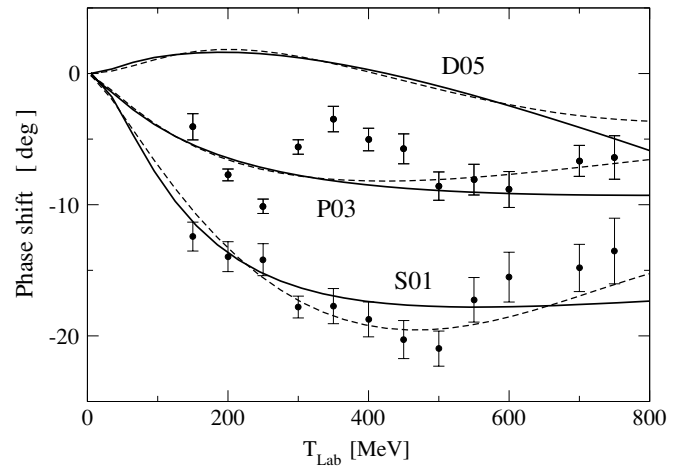


FIG. 1. The isospin-zero stretched states phase shifts as a function of the K^+ kinetic energy. The single- and continuous-energy solutions of the GWU analyses are represented with large and small circles. The solid curves represent the phase shifts from the reference potential.

are short range with significant strengths limited to $r < 1$ fm. The very short range behavior depends on the high-energy extrapolation of the rational function, which we performed as sensibly as possible.

The separable potential functions are motivated and tuned to a short-range zone in which resonances, inelastic scattering, and reactions are supposed to occur [12], for example,

$$\phi_\alpha(r) = N_\alpha r^L \exp[-(r - r_0)^2/a^2], \quad (20)$$

where we have used $r_0 = 0.5$ fm and $a = 0.2$ fm, with N_α a normalization constant.

Any identification of resonances and reaction channels is not part of this endeavor. Thus, the separable term strengths $\Gamma_\alpha(E)$ are fixed to the continuous-energy-solution partial-wave phase shifts [14], whose real phase shifts are shown as dashed curves in Figs. 1–4. Vanishing imaginary phase shifts are limited to the channels S01, P03, D05, and F07.

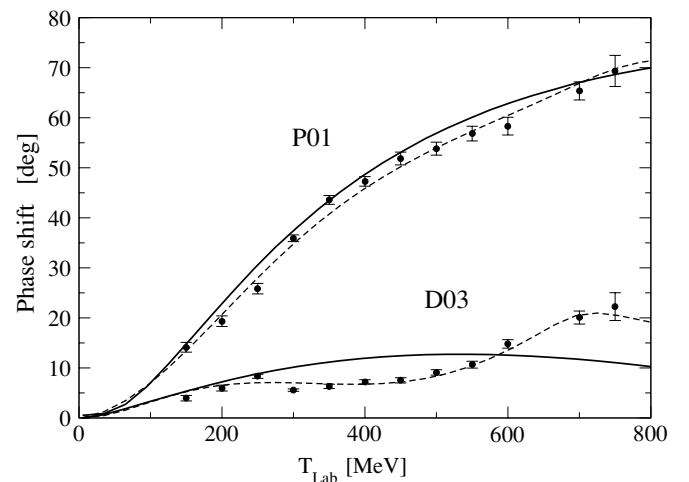


FIG. 2. The same as Fig. 1 but for the unstretched states.

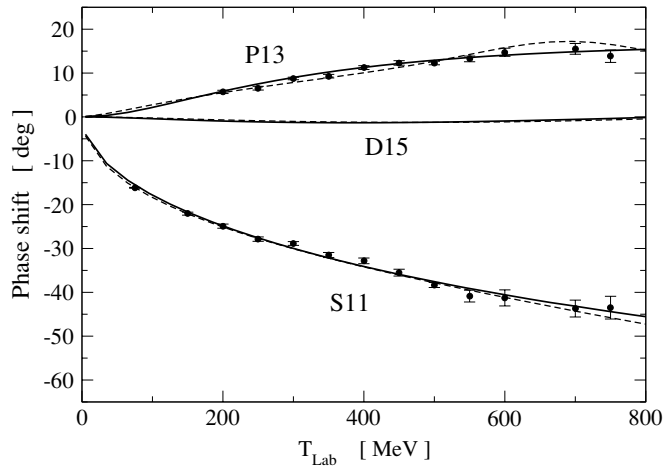


FIG. 3. The isospin-one stretched states phase shifts as a function of the K^+ kinetic energy. The single- and continuous-energy solutions of the GWU analyses are represented with large and small circles. The solid curves represent the phase shifts from the reference potential.

III. THE KA OPTICAL POTENTIAL

An OMP represents an effective single-particle interaction potential for a projectile caused by the interaction with target nucleons. The underlying many-body problem in Brueckner's many-body theory yields an OMP in the form of a convolution of a projectile-nucleon effective interaction, the reaction matrix, with the target mixed density.

There are many practical ways to obtain a successful representation of the effective interaction and its accurate use in the convolution integral. Here we use the KN t -matrix operator, on and off shell, as the effective interaction. Such a construction has successfully been used in the past and we recall only its salient features to make the discussion of various results comprehensible. In the projectile-nucleus c.m. reference frame, the collision of a projectile of kinetic energy E is described by the full-folding OMP, which in a momentum

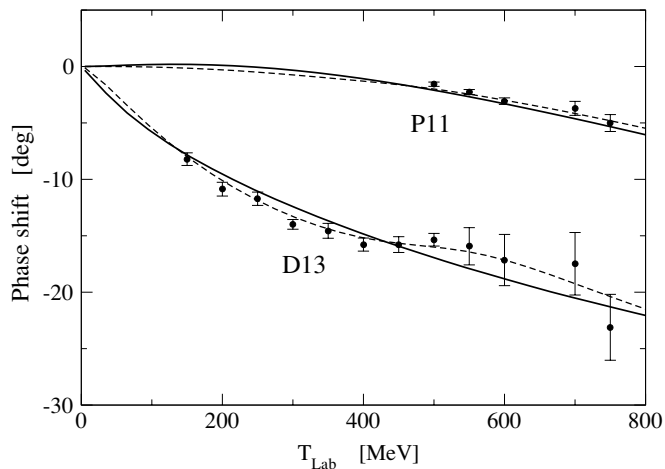


FIG. 4. The same as Fig. 3 but for the unstretched states.

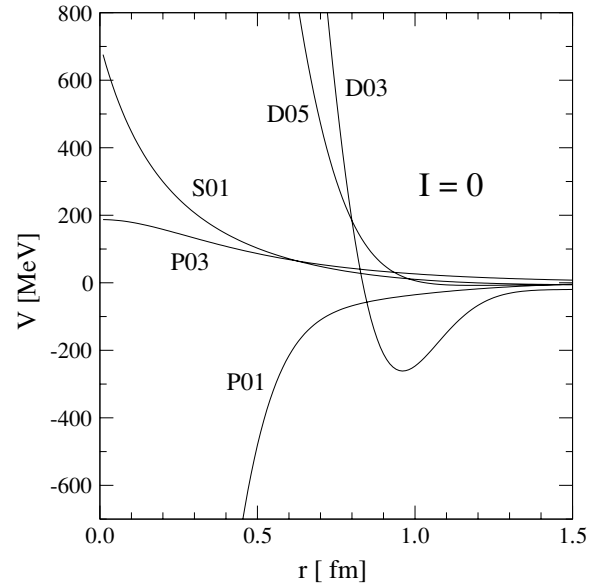


FIG. 5. The radial dependence of the isospin-zero KN reference potentials.

representation is given by [13]

$$U(\mathbf{k}', \mathbf{k}; E) = \sum_{N=p,n} \int d\mathbf{P} \rho_N \left(\mathbf{P} + \frac{\mathbf{q}}{2}, \mathbf{P} - \frac{\mathbf{q}}{2} \right) \times t_{NK^+}(\mathbf{k}_r', \mathbf{k}_r; \mathbf{K} + \mathbf{P}; s), \quad (21)$$

where we define the mean momentum $\mathbf{K} = (\mathbf{k}' + \mathbf{k})/2$ and momentum transfer $\mathbf{q} = \mathbf{k}' - \mathbf{k}$. Here the effective interaction, in the form of the free scattering t matrix, exhibits an explicit dependence on the relative momenta \mathbf{k}_r and \mathbf{k}_r' , the total pair momentum $\mathbf{Q} = \mathbf{K} + \mathbf{P}$, and the pair- s invariant. In particular,

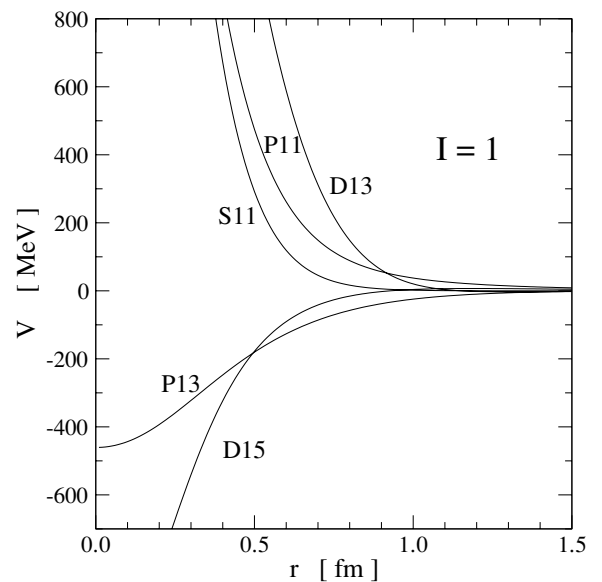


FIG. 6. The radial dependence of the isospin-one KN reference potentials.

the relative momenta take the general form

$$\mathbf{k}_r = W\mathbf{k} - (1 - W)\mathbf{p}, \quad \mathbf{k}'_r = W'\mathbf{k}' - (1 - W')\mathbf{p}', \quad (22)$$

where W and W' are scalar functions of the momenta of the colliding particles with relativistic kinematics built in. Explicit expressions for these quantities have been given in Ref. [13] and are summarized as follows. Let ω and ε be the kaon and nucleon on-shell energies (i.e., $\omega = \sqrt{m_K^2 + \mathbf{k}^2}$ and $\varepsilon = \sqrt{m_N^2 + \mathbf{k}^2}$), respectively. Then W is given by

$$W = \frac{\varepsilon + \varepsilon_r}{\varepsilon + \varepsilon_r + \omega + \omega_r}, \quad (23)$$

with ε_r and ω_r the on-shell relative energies

$$\omega_r = \sqrt{m_K^2 + \mathbf{k}_r^2}, \quad \varepsilon_r = \sqrt{m_N^2 + \mathbf{k}_r^2}. \quad (24)$$

Here the magnitude of the relative momentum is obtained from

$$\mathbf{k}_r^2 = \frac{1}{4s_{\text{in}}} \xi^2(s_{\text{in}}, m_K^2, m_N^2), \quad (25)$$

where the ξ function corresponds to

$$\xi(x, y, z) = \sqrt{(x - y - z)^2 - 4yz}, \quad (26)$$

and the incoming s_{in} invariant is given by

$$s_{\text{in}} = (\varepsilon + \omega)^2 - (\mathbf{p} + \mathbf{k})^2. \quad (27)$$

Identical expressions are used for the primed quantities to obtain the outgoing coefficient W' .

The momentum integral $\int d\mathbf{P}$ signals the folding integral. The intricate dependence of the many vector-valued momenta makes the convolution quite complicated and thus the name full-folding approach was coined to signal use of the full expression, as compared to much simpler approximated expressions. Physically, the folding integral accounts for dynamical effects resulting from Fermi motion as modulated by the shape of the target mixed density. For practical reasons we represent the mixed density in terms of the local density $\rho(R)$ via the Slater approximation [18], that is,

$$\rho\left(\mathbf{P} + \frac{\mathbf{q}}{2}, \mathbf{P} - \frac{\mathbf{q}}{2}\right) = \frac{1}{\pi^2} \int_0^\infty R^2 dR j_0(qR) \Theta[\hat{k}(R) - P] \quad (28)$$

with $\hat{k}(R) = [3\pi^2 \rho(R)]^{1/3}$.

The model equation for the t matrix in terms of a reference KN potential in the KN c.m. reference frame takes the form of the Lippmann-Schwinger type, that is,

$$t_{KN}(\mathbf{p}', \mathbf{p}; s) = V_{KN}(\mathbf{p}', \mathbf{p}) + 2\mu \int \frac{d^3k}{(2\pi)^3} \times \frac{V_{KN}(\mathbf{p}', \mathbf{k}) t_{KN}(\mathbf{k}, \mathbf{p}; s)}{k_o^2 + i0^+ - k^2}. \quad (29)$$

Here, the energy invariant s and associated on-shell momentum k_o are determined from $s = (m_K + E + m_N + \bar{\varepsilon}_N)^2 - \mathbf{Q}^2$, where $\bar{\varepsilon}$ is the average binding energy of the target nucleons and \mathbf{Q} corresponds to the total pair momentum in the KA c.m. frame. The potential V_{KN} is constructed following the inversion procedure described in the previous section. The calculation of the t matrix on and off shell at various energies

follows standard numerical procedures. In the boost of the t matrix from the c.m. to the laboratory reference frame we have included the corresponding Jacobian (or Møller factor) [13].

Although full-folding OMPs were developed in the 1980s for pion as well as nucleon scattering, most K^+ -nucleus scattering analyses continue being made within an on-shell $t\rho$ approximation. We select and discuss three of these factorized forms in this study.

(a) *Off-shell $t\rho$* : A first reduction to a $t\rho$ form emerges after setting $\mathbf{P} = 0$ in the t matrix in Eq. (21), thus allowing the integration of the mixed density over the momentum \mathbf{P} . Hence,

$$U(\mathbf{k}', \mathbf{k}; E) = \sum_{N=p,n} \rho_N(\mathbf{q}) t_{NK^+}(\mathbf{k}', \mathbf{k}; \mathbf{K}; s), \quad (30)$$

where $\rho_N(\mathbf{q})$ represents nuclear density in momentum space. In this factorized form the relative momenta \mathbf{k}_r and \mathbf{k}'_r lie generally off shell, as no constraints on \mathbf{k} or \mathbf{k}' are in place. This reduction is referred to as an off-shell $t\rho$ approximation and has been extensively applied in nucleon-nucleus scattering. An additional further step can be taken to force the t matrix on shell. Quite generally, features at the t -matrix level dictated by four independent variables (two magnitudes, angle, and energy) are specified by two of its arguments, one angle and one energy. We have found that on-shell $t\rho$ results for K^+A scattering depend, albeit moderately, on the prescription used and we focus on two of them.

(b) *On-shell $t\rho$ of the s type*: This is the usual form of the on-shell $t\rho$ approximation and has been applied extensively in hadron-nucleus collisions. We have designated it of the s type since it privileges the energy argument in the t matrix. Basically, the energy \sqrt{s} of the K^+N pair is determined in the Breit frame with the subsequent determination, on shell, of the relative momenta. Details can be found in Ref. [19].

(c) *On-shell $t\rho$ of the k type*: An alternative prescription, which we refer to as of the k type, emerges naturally after considering a series expansion of $U(\mathbf{k}, \mathbf{k}')$ in terms of the magnitudes k and k' around the on-shell momentum k_A in the projectile-nucleus c.m. Then, to lowest order we get

$$U(\mathbf{k}', \mathbf{k}) \approx U(k_A \hat{\mathbf{k}}', k_A \hat{\mathbf{k}}). \quad (31)$$

As a result, the two relative momenta in the t matrix [c.f. Eq. (22)] become equal in magnitude. The pair energy \sqrt{s} is obtained on shell from these relative momenta.

IV. APPLICATIONS AND RESULTS

We focus our applications on differential and total cross sections at kaon momenta in the range 400–1000 MeV/c by considering ${}^6\text{Li}$, ${}^{12}\text{C}$, ${}^{28}\text{Si}$, and ${}^{40}\text{Ca}$ targets. The ground-state densities of the first three targets were obtained from the nuclear charge density fit to electron scattering [20–22]. The point densities were obtained by unfolding the electromagnetic size of the proton from the charge density. In these cases we assume neutron densities equal to the proton densities. In the case of ${}^{40}\text{Ca}$ we have used the densities from Ref. [23].

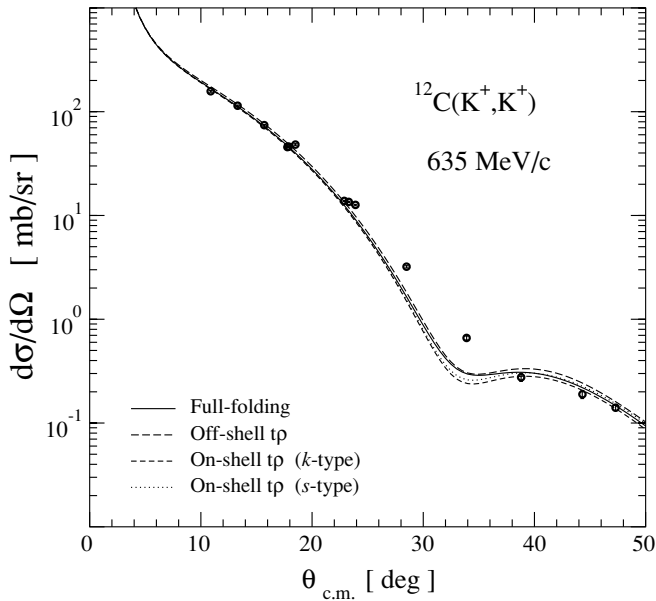


FIG. 7. Differential cross section for $K^+ + {}^{12}\text{C}$ elastic scattering at $P_{\text{Lab}} = 635 \text{ MeV}/c$. The solid curve represents the full-folding results, the long dashed curve corresponds to the off-shell $t\rho$ results. The on-shell $t\rho$ results of k and s type are shown with short-dashed and dotted curves, respectively. The data are from Ref. [24].

The scattering is analyzed within the full-folding OMP and comparisons are made with off- and on-shell $t\rho$ approximations. Thus, we include in the best possible way the off-shell effects in the effective interaction and switch them partially or fully off in the simpler $t\rho$ OMP.

The KA optical potentials are calculated in momentum space following Ref. [13]. The KA S matrix and derived quantities linked with observables are obtained by solving an OMP Lippmann-Schwinger equation in coordinate space for any of the specified nonlocal potentials in the presence of the Coulomb interaction. Furthermore, relativistic kinematics

is used to specify the correct on-shell momentum and corresponding KA reduced energy needed for the Green's function.

In Fig. 7 we show the calculated differential cross section for $K^+ + {}^{12}\text{C}$ scattering at beam momentum $635 \text{ MeV}/c$ with data [24]. The solid curves are the full-folding results, whereas the long-dashed curves are the off-shell $t\rho$ results. The on-shell $t\rho$ results of s and k type are shown as short-dashed and dotted curves, respectively. Although differences exist among all four results, they are quite small. The differences among all $t\rho$ are a measure of the off-shell contributions. The off-shell $t\rho$ results show a uniform shift upward when compared with the full-folding results. More obvious, but still marginal, are differences among the results for scattering angles above 30° .

Similar applications are shown in Fig. 8, where we present the differential cross section for scattering from ${}^6\text{Li}$, ${}^{12}\text{C}$, and ${}^{40}\text{Ca}$ at beam momenta of 715 and $800 \text{ MeV}/c$. The data are taken from Refs. [25,26] and the curve designations follow the convention of Fig. 7. Here again we evidence moderate differences among all four approaches, being visible, at best, for angles above 25° . The comparison with data shows for ${}^6\text{Li}$ (upper left frame) an overestimation of the theory with respect to the data by a factor of ~ 1.8 around 10° . We interpret this discrepancy as being caused by uncertainties in the data normalization. The work by Chen *et al.* [6] shows that they had a similar problem with ${}^6\text{Li}$. In their study they include a phenomenological second-order potential proportional to a power of the nuclear density. They fit the complex strength and power of the density to the data, obtaining results in close resemblance to ours. Overall, the results for ${}^{12}\text{C}$ and ${}^{40}\text{Ca}$ shown in Fig. 8 are in good accord with the data. In the case of ${}^{12}\text{C}$ at $715 \text{ MeV}/c$ (lower left frame) some differences between theory and data, at angles above 30° are present. The full-folding and any of the $t\rho$ approaches are remarkably similar for differential cross sections.

Total cross sections for K^+ -nucleus collisions have been extracted from transmission experiments [1,2,4]. Such data are complementary to the differential cross section data and

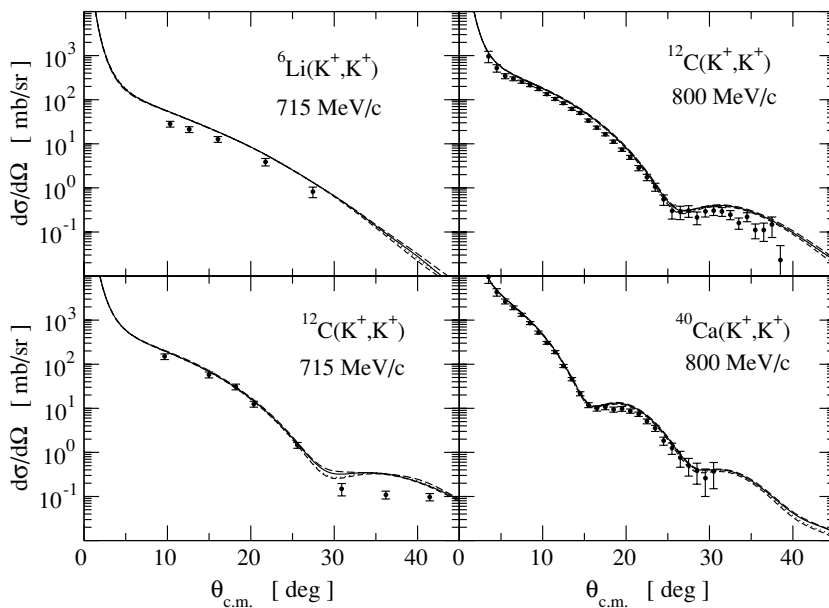


FIG. 8. Differential cross section for elastic scattering of K^+ from ${}^6\text{Li}$ (upper left frame), ${}^{12}\text{C}$, and ${}^{40}\text{Ca}$ (lower right frame) at beam momenta of $715 \text{ MeV}/c$ (left frames) and $800 \text{ MeV}/c$ (right frames). The curve patterns are the same as in Fig. 7. The data at 715 and $800 \text{ MeV}/c$ are from Refs. [25] and [26], respectively.

often exhibit larger differences among the full-folding and $t\rho$ results, even though the same KN effective interaction is used. Before jumping to premature conclusions about the effective interaction or the quality of any of the theoretical models, it is important to remember that the transmission total cross sections σ_T have their own model dependence built into the data. This has been discussed in some detail elsewhere [27,28]. Using $\sigma_T(\Omega)$ as the experimentally measured transmission cross section, subtending a solid angle Ω from the target along the beam axis, we obtain a total cross section of

$$\sigma_T = \lim_{\Omega \rightarrow 0} [\sigma_T(\Omega) - \sigma_C(\Omega_>) - \sigma_{CN}(\Omega_>) + \sigma_N(\Omega_<) + \sigma_I(\Omega_<)], \quad (32)$$

where $\Omega_>$ and $\Omega_<$ refer to the integrated cross section outside and inside the solid angle Ω , respectively. Furthermore, we use the following nomenclature for particular cross sections: $\sigma_C(\Omega_>)$ for the point charge Coulomb cross section, $\sigma_{CN}(\Omega_>)$ for the Coulomb and nuclear interaction interference term, $\sigma_N(\Omega_<)$ for the nuclear cross section from the nuclear interaction, and $\sigma_I(\Omega_<)$ for that arising from inelasticities. In the limit $\Omega \rightarrow 0$ the last two terms vanish. However, σ_{CN} requires very accurate results for the nuclear plus Coulomb interaction amplitude. This requires knowledge and availability of a high-quality optical model in the first place; this introduces a model dependence of σ_T that is beyond our judgment and puts limits on our conclusions. Nevertheless, we have calculated the total cross sections with all four optical models discussed here and we compare the results with data reductions presented by Friedman *et al* [1] and by Friedman, Gal, and Marš [2]. The difference between the data reported in these two references lies in the way the optical potential, in a $t\rho(r)$ form, is constructed to extract the total cross sections from transition experiments. Whereas in Ref. [1] the $t\rho$ form is based on a density-independent t -matrix strength, in Ref. [2] the imaginary part of the strength exhibits a parametric density dependence adjusted to yield, self-consistently, the total cross sections. Thus, the data reported in the second reference are consistent within an empirical medium dependence (c.f. Eq. (5) of Ref. [2]) of the t matrix and reflect, to some extent, the model dependence of their reported measurements.

In Figs. 9 and 10 we present the ratios of experimental to calculated reaction cross sections $\sigma_R(\text{Exp.})/\sigma_R(\text{Calc.})$ and the total cross sections $\sigma_T(\text{Exp.})/\sigma_T(\text{Calc.})$ for four target nuclei at four projectile momenta. Notice that all ratios are nearly constant as a function of projectile momentum, whereas only the ${}^6\text{Li}$ results lie somewhat below the other three cases. Quite similar results are obtained by considering the other three forms of the $t\rho$ model. When comparing Figs. 9 and 10 we observe a clear shift in the reaction cross section of the latter with respect to the former. This shift is consistent with the rescaling of the imaginary part of the strength of the t matrix used in the construction of the optical potential [2]. The question is, therefore, whether this prescription to incorporate medium corrections effectively accounts for genuine medium effects in the form of short range-correlations, Fermi motion, and their implied nonlocal effects in the K^+ -nucleus coupling. An assessment of these issues has yet to be made.

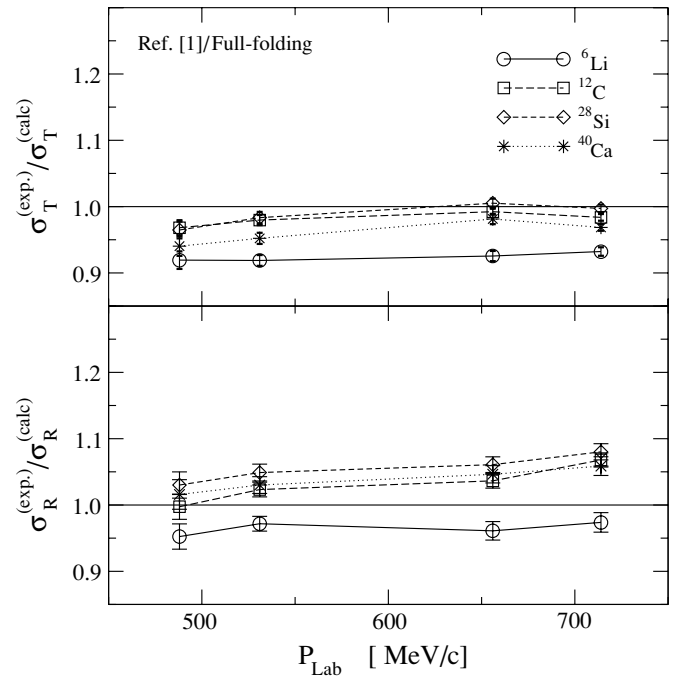


FIG. 9. Experimental-to-calculated ratios for the total (σ_T) and reaction (σ_R) cross sections for K^+ elastic scattering from ${}^6\text{Li}$, ${}^{12}\text{C}$, ${}^{28}\text{Si}$, and ${}^{40}\text{Ca}$ at 488, 531, 656, and 714 MeV/c. Results are based on the full-folding approach. Connecting lines have been drawn to guide the eye. The data are taken from Ref. [1].

The features observed in the figures can also be seen in Table I, where we present the measured and calculated cross sections at four momenta for the selected targets from calculations based on the four approaches discussed here. For instance, the results shown in Fig. 9 correspond to the ratios

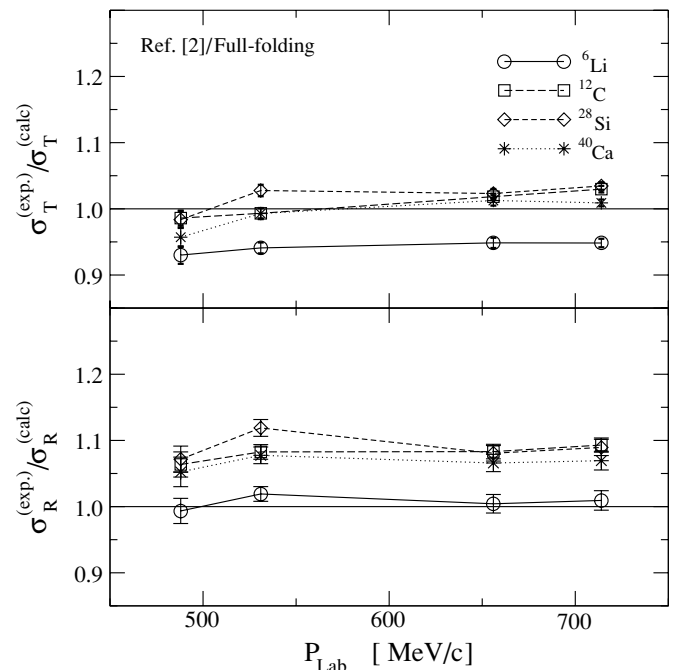


FIG. 10. The same as Fig. 9, but with data taken from Ref. [2].

TABLE I. Experimental and calculated reaction and total cross sections (in millibarns) for K^+ -nucleus scattering at the specified momenta. The data in the first and second block are from Refs. [1,2] with corresponding errors in parentheses.

Source	P_{Lab} [MeV/c]	Reaction				Total			
		${}^6\text{Li}$	${}^{12}\text{C}$	${}^{28}\text{Si}$	${}^{40}\text{Ca}$	${}^6\text{Li}$	${}^{12}\text{C}$	${}^{28}\text{Si}$	${}^{40}\text{Ca}$
Data [1]	488	65.0(1.3)	120.4(2.3)	265.5(5.1)	349.9(7.7)	76.6(1.1)	162.4(1.9)	366.5(4.8)	494.4(7.7)
	531	69.8(0.8)	129.3(1.4)	280.4(3.4)	367.1(4.5)	78.8(0.7)	166.6(1.3)	374.8(3.3)	500.2(4.4)
	656	75.6(1.1)	141.8(1.5)	306.1(3.4)	401.1(5.0)	84.3(0.7)	174.9(0.8)	396.1(2.7)	531.9(4.2)
	714	79.3(1.2)	149.3(1.5)	317.5(3.6)	412.9(5.5)	87.0(0.6)	175.6(0.9)	396.5(2.3)	528.4(2.8)
Data [2]	488	67.8(1.3)	128.4(2.3)	276.2(5.1)	362.5(7.7)	77.5(1.1)	165.4(1.9)	373.7(4.8)	503.2(7.7)
	531	73.2(0.8)	136.8(1.4)	299.1(3.4)	384.0(4.5)	80.7(0.7)	168.9(1.3)	391.7(3.3)	521.6(4.4)
	656	79.0(1.1)	148.2(1.5)	311.8(3.4)	408.6(5.0)	86.4(0.7)	179.5(0.8)	403.2(2.7)	548.8(4.2)
	714	82.2(1.2)	152.8(1.5)	320.2(3.6)	417.1(5.5)	88.5(0.6)	183.8(0.9)	411.3(2.3)	550.4(2.8)
Full-folding	488	68.2	120.7	257.7	344.4	83.3	167.7	379.9	525.8
	531	71.8	126.4	267.3	356.4	85.8	170.1	381.2	525.4
	656	78.7	136.8	288.5	383.3	91.1	176.3	394.1	542.0
	714	81.4	139.8	293.9	390.0	93.3	178.5	397.6	545.5
Off-shell $t\rho$	488	70.1	124.8	265.1	353.7	86.3	175.8	396.5	548.4
	531	73.5	129.9	274.0	364.7	88.3	176.9	395.7	545.3
	656	79.9	139.6	293.0	388.7	92.9	181.2	403.2	554.0
	714	83.0	141.9	298.2	395.2	94.7	182.5	405.8	556.3
$t\rho$ k type	488	67.7	118.5	252.4	336.8	82.7	164.4	369.3	508.5
	531	71.2	124.1	262.7	349.8	85.0	166.4	371.6	510.3
	656	78.3	135.0	284.9	378.4	90.5	173.4	386.8	530.8
	714	80.3	138.6	291.3	386.2	92.2	176.3	391.5	535.9
$t\rho$ s type	488	69.2	122.6	260.4	347.4	84.9	170.9	382.9	527.6
	531	72.7	128.0	270.2	359.7	87.0	172.2	383.6	527.0
	656	79.5	138.3	291.1	386.6	92.0	177.6	395.9	543.5
	714	81.4	141.6	297.1	393.8	93.4	180.1	399.7	547.4

between the first two blocks of this table. When comparing the full-folding cross sections with the on-shell $t\rho$ results, we observe that the former lies systematically above the k type, but it has below the s type. These differences may be used to estimate the off-shell sensitivity, which we estimate as $\pm 3\%$

for the worst case. The off-shell $t\rho$ result is always above the other three results and its difference to the data is the largest.

The features already observed become more evident in Fig. 11, where we present the measured and calculated reaction

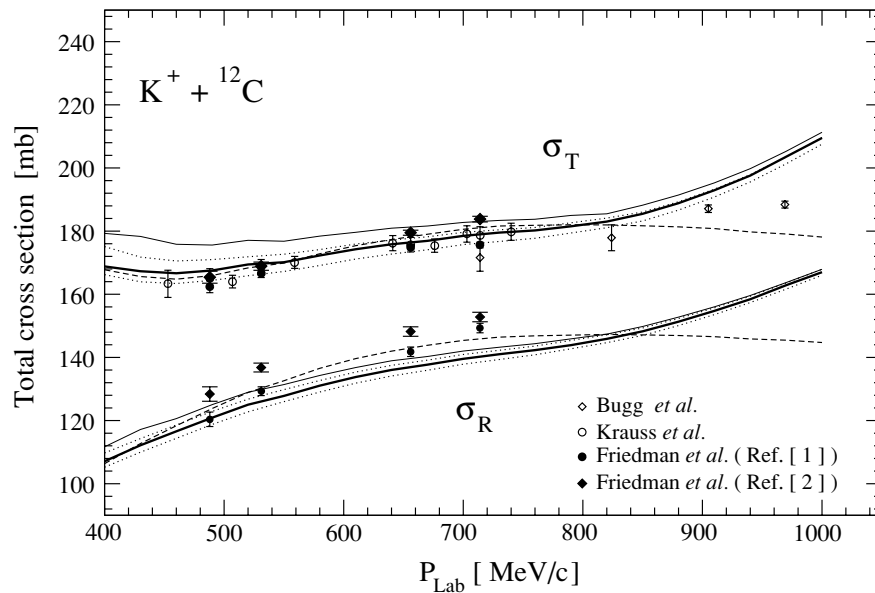


FIG. 11. Measured and calculated total cross sections as functions of the beam momentum for $K^+ + {}^{12}\text{C}$ scattering. The thick curves represent full-folding results; the dotted and thinner solid curves correspond to on- and off-shell $t\rho$ results, respectively. The dashed curves represent full-folding results with the separable strength of the elemental KN potential suppressed. The data are from Refs. [1,2,4,29].

σ_R and total σ_T cross sections for ^{12}C as a function of the kaon momentum, in the range 400–1000 MeV/c. The data from Bugg *et al.* [29] and Krauss *et al.* [4] are shown with open diamonds and circles, respectively. The data from Friedman *et al.* [1] and Friedman, Gal, and Marčs [2] are shown with black circles and diamonds, respectively. Here, the thicker solid curves represent the full-folding results, whereas the dotted ones are based on the on-shell $t\rho$ approaches. The off-shell $t\rho$ results are shown with the thinner solid curves. Finally, we present full-folding results when only the reference inversion potentials are used in the KN effective interaction, thereby completely suppressing the separable contribution. These results for σ_T and σ_R are shown with dashed curves.

The full-folding and on-shell $t\rho$ approximations give an overall reasonable agreement (within 5%) with the measured total cross sections up to 900 MeV/c, above which they depart from the data. Notice that an agreement within error bars is achieved with the data of Krauss *et al.* [4] for ^{12}C (open circles) in the momentum range 400–800 MeV/c. Furthermore, the s -type $t\rho$ σ_T results (upper dotted curves) are in poorer agreement with the data in comparison with the k -type $t\rho$ and full-folding approach, particularly below 500 MeV/c. The different variants of the $t\rho$ approximations near 400 MeV/c yield total cross sections varying between ~ 160 and ~ 180 mb, representing more than 10% of the measured value (20 mb). When only the on-shell approximations are considered these variations diminish to about 5% (10 mb), decreasing at higher momenta. These results illustrate the level of uncertainty implicit in any $t\rho$ approximation when used as representations of the off-shell Fermi-motion integrals of the effective interaction.

A closer scrutiny of the gradual departure of the calculated total cross section relative to the data, above 900 MeV/c, would require the study of possible uncertainties in the elemental KN amplitude and enable an assessment of their impact on total cross sections. These considerations go beyond the focus of the present work. Incidentally, the results in which the separable strength of V_{KN} is suppressed (dashed curves) indicate that, despite marginal differences in the description of the real phase shifts, the absorptive component becomes important in the asymptotic behavior of the cross sections. It is in this high-energy regime where the single- and continuous-energy solutions exhibit sizable differences.

The sensitivity of σ_T to the alternative approaches considered here is somewhat diminished in the context of the reaction cross section, where all curves stay much closer to each other. An interesting feature which emerges after comparing the calculated total and reaction cross sections is their nearly constant difference above 600 MeV/c. In the particular case of ^{12}C we observe

$$\sigma_T \approx \sigma_R + 39 \text{ [mb]}. \quad (33)$$

A similar behavior is exhibited by the other targets, as inferred from Table I.

The study of total cross sections for $N = Z$ nuclei has also been of some interest as a means to gauge the role of medium effects in the propagation of kaons through the nucleus. Weiss and collaborators [30] found that the ratio σ_T/A for ^6Li and

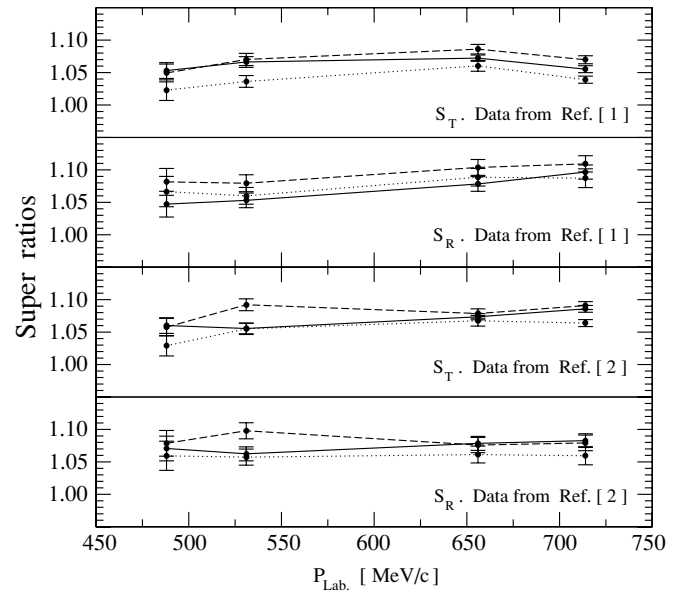


FIG. 12. Super ratios for total and reaction cross sections based on data from Refs. [1,2] and the full-folding approach. The solid, dashed, and dotted curves represent results for ^{12}C , ^{28}Si , and ^{40}Ca , respectively.

deuterium are nearly the same, suggesting that multiple-step contributions are rather weak in these light targets. Such is not the case for the heavier targets. To quantify this feature, Friedman *et al.* have introduced the super ratio, that is, the ratio $\sigma_{\text{Exp.}}(A)\sigma_{\text{Calc.}}(^6\text{Li})/\sigma_{\text{Calc.}}(A)\sigma_{\text{Exp.}}(^6\text{Li})$. Although it is correct that this quantity would diminish normalization uncertainties, its departure from unity may indicate not only medium effects but also the level of disagreement between theory and experiment. Indeed, their reported values for each target exhibit distinctive curves as function of the momentum, with values ranging between 1.15 and 1.25. Although limited by the fact that the optical model used to extract the data in Refs. [1,2] differs from the full-folding model used here, we have also calculated the super ratios using the results in Table I. In Fig. 12 we plot the total (S_T) and reaction (S_R) super ratios using the data from Ref. [1] (upper two frames) and Ref. [2] (lower two frames) against the full-folding results. Notice that all super ratios are nearly constant as functions of the momentum, with variations between 1.0 and 1.1, consistent with the level of agreement shown in Figs. 9 and 10. Nonetheless, definitive analyses of these super ratios require the use of full-folding KA optical potentials to extract the cross-section data from transmission experiments, an endeavor beyond the scope of this work.

V. CONCLUSIONS

We have studied K^+ -nucleus elastic scattering from light nuclei in the momentum range 400–1000 MeV/c within the full-folding optical model potential framework. To this purpose we have used the t matrix based on a KN potential model with absolute match of the phase-shift analyses reported by the GWU group. The emphasis here has been placed on a

strict connection between the bare KN potential (consistent with the current phase-shift analysis) and the K^+ -nucleus scattering process. This feature is achieved by adding a separable term to a local reference potential obtained within the Gel'fand-Levitant-Marchenko quantum inversion. The t matrix, based on this bare potential model, is convoluted with the nuclear mixed density, leading to a nonlocal KA optical potential. The scattering observables were compared with those obtained within off-shell and two alternative versions of on-shell $t\rho$ approximations, which we have designated as of s and k type, respectively. We observe moderate log-scale differences in differential cross sections among the calculated results from all four approaches. With regard to reaction and total cross sections from transmission experiments, we observe a 10–20% sensitivity arising from the way the Fermi motion is approximated in the different $t\rho$ variants examined here for $P_{\text{Lab}} \lesssim 700$ MeV/c. Considering the full-folding model approach, the results for ^{12}C exhibit a near complete agreement, within error bars, with the total cross sections reported by Krauss *et al.* [4] at momenta between 450 and 750 MeV/c. Such agreement is not observed with the data reported by Friedman and collaborators for ^{40}Ca , ^{28}Si , ^{12}C , and ^6Li . Although the level of agreement observed in these cases remains within 10%, clear discrepancies are observed (c.f. Figs. 9 and 10).

The possible manifestation of the $\Theta^+(1540)$ pentaquark in the collision of K^+ with nuclei has been the subject of recent interest [10]. Indeed, it has been reported that the addition of a quadratic functional of the density to a local $t\rho$ -like optical

potential, $b_o\rho(r) \rightarrow b_o\rho(r) + B\bar{\rho}\rho(r)$, enables a substantial improvement in the fits of transmission-experiment total cross sections data in KA scattering. Additionally, this phenomenological quadratic term, introduced as a means to represent the loss of flux owing to $K^+nN \rightarrow \Theta^+N$ two-nucleon absorption, has been used by the authors of Ref. [10] to predict submillibarn cross section for Θ^+ production on deuterium. From a different prospective, Tolós and collaborators [31] have recently reported on the influence of $\Theta^+(1540)$ degrees of freedom in the context of the single-particle potential of kaons in nuclear matter. In their study special emphasis has been placed on the inclusion of Fermi motion and Pauli blocking effects in the self-consistent determination of the mass operator. It is found that “ $T\rho$ ” representations of the self-consistent potentials differ significantly from those where Fermi motion and Pauli blocking are fully accounted for, and it is observed that Θ^+ pentaquarks affect the self-consistent potentials up to 20% for the real part and $\sim 30\%$ for its width. The implications of these *in-medium* effects in the context of a microscopic description of KA scattering remain to be investigated.

ACKNOWLEDGMENTS

H.F.A. acknowledges the Nuclear Theory Group of the University of Hamburg for its kind hospitality during his visit. Partial funding for this work was provided by FONDECYT under Grant No. 1040938.

-
- [1] E. Friedman *et al.*, Phys. Rev. C **55**, 1304 (1997).
 - [2] E. Friedman, A. Gal, and J. Marš, Nucl. Phys. **A625**, 272 (1997).
 - [3] L. K. Kerr, B. C. Clark, S. Hama, L. Ray, and G. W. Hoffmann, Prog. Theor. Phys. **103**, 321 (2000), and references therein.
 - [4] R. A. Krauss *et al.*, Phys. Rev. C **46**, 655 (1992).
 - [5] Y. Mardor *et al.*, Phys. Rev. Lett. **65**, 2110 (1990).
 - [6] C. M. Chen, D. J. Ernst, and M. B. Johnson, Phys. Rev. C **59**, 2627 (1999).
 - [7] J. C. Caillon and J. Labarsouque, Nucl. Phys. **A589**, 609 (1995).
 - [8] J. C. Caillon and J. Labarsouque, Phys. Rev. C **53**, 1993 (1996).
 - [9] M. F. Jiang, D. J. Ernst, and C. M. Chen, Phys. Rev. C **51**, 857 (1995).
 - [10] A. Gal and E. Friedman, Phys. Rev. Lett. **94**, 072301 (2005).
 - [11] M. Sander and H. V. von Geramb, Phys. Rev. C **56**, 1218 (1997).
 - [12] A. Funk, H. V. von Geramb, and K. A. Amos, Phys. Rev. C **64**, 054003 (2001).
 - [13] H. F. Arellano and H. V. von Geramb, Phys. Rev. C **66**, 024602 (2002).
 - [14] R. A. Arndt, W. J. Briscoe, R. L. Workman, and I. I. Strakovsky, CNS DAC [SAID], Physics Dept., George Washington University, <http://gwddac.phys.gwu.edu>. Current K^+N solution as of November 4, 2004.
 - [15] J. S. Hyslop, R. A. Arndt, L. D. Roper, and R. L. Workman, Phys. Rev. D **46**, 961 (1992).
 - [16] H. W. Crater and P. Van Alstine, J. Math. Phys. **31**, 1998 (1990).
 - [17] B. Liu and H. Crater, Phys. Rev. C **67**, 024001 (2003).
 - [18] H. F. Arellano, F. A. Brieva, and W. G. Love, Phys. Rev. C **42**, 652 (1990).
 - [19] M. J. Páez and R. H. Landau, Phys. Rev. C **24**, 1120 (1981).
 - [20] G. C. Li, R. R. Whitney, and M. R. Yearian, Nucl. Phys. **A162**, 583 (1971).
 - [21] I. Sick and J. S. McCarthy, Nucl. Phys. **A150**, 631 (1970).
 - [22] G. C. Li, I. Sick, and M. R. Yearian, Phys. Lett. **B37**, 282 (1971).
 - [23] J. W. Negele, Phys. Rev. C **1**, 1260 (1970).
 - [24] R. E. Chrien, R. Sawafra, R. J. Peterson, R. A. Michael, and E. V. Hugerford, Nucl. Phys. **A625**, 251 (1996).
 - [25] R. Michael *et al.*, Phys. Lett. **B382**, 29 (1996).
 - [26] D. Marlow *et al.*, Phys. Rev. C **25**, 2619 (1982).
 - [27] W. B. Kaufmann and W. R. Gibbs, Phys. Rev. C **40**, 1729 (1989).
 - [28] M. Arima and K. Masutani, Phys. Rev. C **47**, 1325 (1993).
 - [29] D. V. Bugg *et al.*, Phys. Rev. **168**, 1466 (1968).
 - [30] R. Weiss *et al.*, Phys. Rev. C **49**, 2569 (1994).
 - [31] L. Tolós, A. Ramos, and A. Polls, arXiv: hep-ph/0503009.